A Study on the Parameter Estimation of DURUMI-II for the Fixed Right Elevator Using Flight Test Data

Wook-Je Park*, Eung-Tai Kim, Kie-Jeong Seong
Korea Aerospace Research Institute,
P.O. BOX 113, Yuseong, Daejeon 305-600, Korea
Yeong-Cheol Kim
Agency for Defense Development,
P.O. BOX 35, Yuseong, Daejeon 305-600, Korea

The stability and control derivatives of DURUMI-II UAV using the flight test are obtained. The flight test data is gathered from the normal flight condition (normal mode) and the flight condition assumed as the right elevator fixed (fault mode). Using real-time parameter estimation techniques, applied to Fourier transform regression method, simulates the aircraft motion. From the result, the fault of control surface is to be detected. In this paper, the results of the real-time parameter estimation techniques are compared with the results of the Advanced Aircraft Analysis (AAA). Using the aerodynamic derivatives, it provides the base line of normal/failure for the control surface by using the on-line parameter estimation of Fourier transform regression. In flight, this approach maybe helpful to detect and isolate the fault of primary control surface. It is explained how to perform the flight condition assumed as the right elevator fixed in the flight test. Also, it is mentioned how to switch between the normal flight condition and the assumed fault flight condition.

Key Words : Fault Detection, Real-Time Parameter Estimation, Flight Test, UAV

Nomenclature

A,B,C,D: System matrices
J : Cost function
x : State vector
y : Response vector
u : Input vector
t : Time, sec
σ : Standard deviation of estimation error
ω : Frequency, rad/sec

Superscripts

r : Transpose
$\sim$: Discrete Fourier transform
-1 : Matrix inverse
$*$: Complex conjugate transpose
$\hat{}$: Estimate

Subscripts

L,D,Y : Lift, Drag, Side force
l,m,n : Rolling, Pitching, Yawing moment
p,q,r : Angular velocities, rad/sec or deg/sec
ϕ,θ,ψ : Roll, Pitch, Yaw angular, deg
α : Angle of attack, deg
β : Sideslip angle, deg
δ : Control surface deflection, rad or deg
e,a,r : Elevator, Aileron, Rudder
i : Value at time
0 : Trim or initial value

* Corresponding Author,
E-mail : twinbee7@paran.com
TEL : +82-42-860-2564; **FAX** : +82-42-860-2009
Korea Aerospace Research Institute, P.O. BOX 113, Yuseong, Daejeon 305-600, Korea. (Manuscript **Received** March 24, 2006; **Revised** May 29, 2006)

1. Introduction

Typically, the Maximum Likelihood Estimation (MLE) (Ljung, 1987) is the most widely used

algorithm for parameter estimation for the aircraft dynamic model from flight test data (Park, 1997; 2004; Hwang, 2001; 2002). The iterative algorithm of the Maximum Likelihood Estimation is slower than the Extended Kalman Filter (EKF) or the Fourier Transform Regression (FTR) algorithm. The Extended Kalman Filter (Garcia-Velo, 1991; 1997; Gelb, 1974; Mendel, 1987) is basically a state estimation, which is the same as the direct parameter estimation. The Extended Kalman Filter is one-pass algorithm, which means that it is faster than the MLE algorithm and can be applied to the unstable and on-line systems. The Fourier transform 15 (Morelli, 1997; 1998; 1999; 2000; Napolitano, 2001; Song, 2001) is proposed for the parameter estimation algorithm. It consists of suitably excited input and actually measured system responses, therefore it is possible to be repeatedly implemented to an UAV test aboard in real time. Both of the FTR and EKF are applicable to on-line parameter estimation.

The FTR algorithm is preferably applied, because of its fast convergence and robustness to measurement and system noise while The EKF has the problem of sensitivity on initial values. Recently, The FTR is applied to the parameter estimation of an aircraft which experiences failure or damage state as well as normal state. For enhance the flight safety during failure mode test, the DURUMI-II, a research UAV developed by KARI, are designed to have redundancy in the control surface. The selection of flight mode between normal and failure state is remotely performed by handling switches during flight test.

2. Flight Test for the Normal and Fault of Control Surface

2.1 Control surface redundancy of DURUMI-II

Figure 1 shows the developed DURUMI-II in landing. The Specifications of DURUMI-II are presented in Table 1.

To realize the flight condition assumed as the right elevator fixed and other control surface fault, the control surfaces, elevator and ailerons, DURUMI-II are respectively split into two pieces

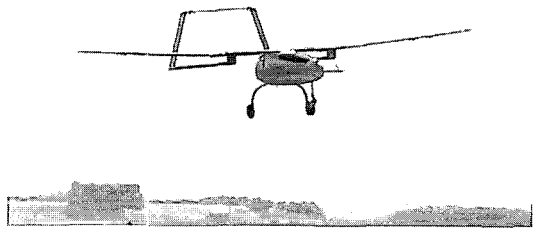

Fig. 1 DURUMI-II in Landing

Table 1 DURUMI-II Specifications

Overall length, m	2.7
Overall height, m	1.22
Main wing span, m	4.8
Aspect Ratio	15
Powerplant	ZDZ 80RV
Power, hp	7.9
Maximum speed, km/h	150
Cruise speed, km/h	125
Stall speed, km/h	60
Maximum take-off weight, kg	37
Empty weight, kg	22
Payload, kg	12

and rudder is added. Figs. 2 and 3 show the changed configuration of DURUMI-II. This system will help DURUMI-II to fly safely, if any malfunction of control surface should occur. The selection of flight mode between normal and failure state is remotely performed by handling switch during the flights.

2.2 Flight test of DURUMI-II and input design

In the flight condition assumed as the right elevator fixed, DURUMI-II has been tested to obtain aerodynamic coefficients and control derivatives using real-time parameter estimation method such as Fourier transform regression. In the flight test of DURUMI-II, the multi-step 3-2-1-1 input (NTPS, 2000) would produce the best response of DURUMI-II, with the greatest amount of information about the aircraft dynamics, for the determination of the best set of stability and

Table 2 Fault assumed flight test condition

Normal Mode	2-1-1 & 3-2-1-1 Input at throttle 50%
Fault Mode I (Right Elevator Fixed : 0 deg)	3-2-1-1 Input at throttle 50%
Fault Mode II (Right Elevator Fixed : +5 deg)	3-2-1-1 Input at throttle 50%

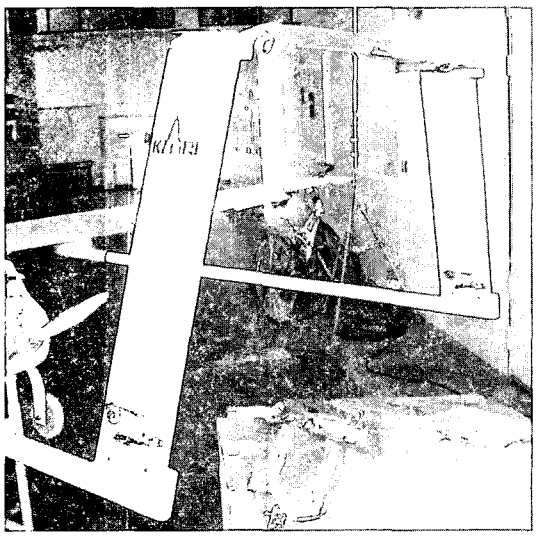

Fig. 2 Split in elevator and addition in rudder

Fig. 3 Split of Ailerons

control derivatives. The control input of amplitude excursion has been programmed in R/C transmit device. The flight test engineer who is independent of ground test pilot remotely executes the control input. In order to realize fault flight, the right elevator fault occurs by operating the switch and knob in flight, the ground test pilot make a level flight. Keeping steady state condition, the flight test engineer is remotely applied for the control input. Table 2 shows two cases of flight conditions assumed as the right elevator fixed.

In flight, in order to perform the exact control input, it is necessary for the ground test pilot to train for a long time. But, operating the programmed switch solves this problem. The 3-pole switch and extra one channel are necessary for the exact control input (FUTABA, 1995). The neural position of switch is set to zero values of control input, and two end positions of switch are set to +/−5 deg values of control input. The extra channel is mixed with control input such as an elevator, ailerons, and rudder. Also, in order to perform of switching for normal state and fault state assumed as the right elevator fixed, the 2-pole switch is operated on the on/off function, so-called program mixing on/off function. This programming method is an epoch-making event to reduce the cost, the time, and the effort.

3. Modeling Formulation

Airplane dynamics can be described by the following linear modeling equations :

$$\dot{x}(t) = Ax(t) + Bu(t) \tag{1}$$

$$y(t) = Cx(t) + Du(t) \tag{2}$$

The dynamic system, whose parameters are to be estimated, has stability and control derivatives. The parameters to be estimated are assumed to be constant during the flight test maneuver.

The finite Fourier transform of a signal $x(t)$ is defined by

$$\tilde{x}(\omega) = \int_0^T x(t)\, e^{-j\omega t} dt \tag{3}$$

Applying the Fourier transform to Eqs. (1) and (2) gives

$$j\omega\tilde{x}(\omega) = A\tilde{x}(\omega) + B\tilde{u}(\omega) \tag{4}$$

$$\tilde{y}(\omega) = C\tilde{x}(\omega) + D\tilde{u}(\omega) \tag{5}$$

When the states x, outputs y, and inputs u are measured, individual state or output equations form vector Eqs. (4) or (5) can be used in an equation error formulation to estimate the stability and control derivatives contained in matrices A, B, C, and D.

For the k-th state equation of vector Eq. (4),

the cost function is

$$J_k=\frac{1}{2}\sum_{n=1}^{m}|j\omega_n\tilde{x}(\omega_n)-A_k\tilde{x}(\omega_n)-B_k\tilde{u}(\omega_n)|^2 \quad (6)$$

Similar Cost expressions can be written for Eq. (2)

$$Y=X\Theta+\varepsilon \quad (7)$$

where

$$\begin{bmatrix} j\omega_1\tilde{x}(\omega_1) \\ j\omega_2\tilde{x}(\omega_2) \\ \vdots \\ j\omega_m\tilde{x}(\omega_m) \end{bmatrix}=\begin{bmatrix} \tilde{x}^T(\omega_1),\ \tilde{u}^T(\omega_1) \\ \tilde{x}^T(\omega_2),\ \tilde{u}^T(\omega_2) \\ \vdots \\ \tilde{x}^T(\omega_m),\ \tilde{u}^T(\omega_m) \end{bmatrix}\begin{bmatrix} A_k^T \\ B_k^T \end{bmatrix} \quad (8)$$

and ε represents the equation error in the frequency domain. The least squares cost function is

$$J=\frac{1}{2}(Y-X\Theta)^*(Y-X\Theta) \quad (9)$$

$$\hat{\Theta}=[\mathrm{Re}(X^*X)]^{-1}\mathrm{Re}(X^*Y) \quad (10)$$

The estimated parameter covariance matrix is

$$\begin{aligned}\mathrm{cov}(\hat{\Theta})&=E[(\hat{\Theta}-\Theta)(\hat{\Theta}-\Theta)^{-1}] \\ &=\hat{\sigma}^2[\mathrm{Re}(X^*X)]^{-1}\end{aligned} \quad (11)$$

where the equation error variance $\hat{\sigma}^2$ can n be estimated from the residuals,

$$\hat{\sigma}^2=\frac{1}{(m-p)}[(Y-X\hat{\Theta})^*(Y-X\hat{\Theta})] \quad (12)$$

where p is the number of elements in parameter vector $\hat{\Theta}$.

For a given frequency ω, the discrete Fourier transform at sampling time i-th is defined.

$$X_i(\omega)=X_{i-1}(\omega)+x_ie^{-j\omega_i\Delta t} \quad (13)$$

The quantity $e^{-j\omega_i\Delta t}$ is constant for given frequency and constant sampling interval.

Rigid body dynamics of DURUMI-II lie in the rather narrow frequency band of 0.01-1.5 Hz. It is therefore possible to select closely spaced fixed frequencies for the Fourier transform and the subsequent data analysis. In this work, frequency spacing of 0.02 Hz was founded to be adequate, which gives 50 frequencies evenly distributed on the interval 0.02-1.0 Hz for each transformed time domain signal.

For longitudinal and lateral-directional combining aircraft dynamics, the state vector x, input vector u, and output vector y in Eqs. (1) and (2) are defined by

$$x=[\alpha\ u\ q\ \theta\ \beta\ p\ r\ \phi]^T \quad (14)$$

$$u=\delta_e \quad (15)$$

System matrices containing the model parameters are:

$$A=\begin{bmatrix} A_1 & \vdots & 0 \\ \cdots & & \cdots \\ 0 & \vdots & A_2 \end{bmatrix} \quad (16)$$

$$B=\begin{bmatrix} X_{\delta_e} \\ \dfrac{z_{\delta_e}}{u_0} \\ M_{\delta_e}+\dfrac{M_{\dot{\alpha}}}{u_0}z_{\delta_e} \\ 0 \\ 0 \\ L_{\delta_e} \\ N_{\delta_e} \\ 0 \end{bmatrix} \quad (17)$$

where

$$A_1=\begin{bmatrix} X_u & X_\alpha & 0 & -g\cos\theta_0 \\ \dfrac{Z_u}{u_0} & \dfrac{Z_\alpha}{u_0} & 1 & 0 \\ M_u+\dfrac{M_{\dot{\alpha}}}{u_0}Z_u & M_\alpha+\dfrac{M_{\dot{\alpha}}}{u_0}Z_\alpha & M_q+M_{\dot{\alpha}} & 0 \\ 0 & 0 & 1 & 0 \end{bmatrix} \quad (18)$$

$$A_2=\begin{bmatrix} Y_v & Y_p & Y_r & g\cos\theta_0 \\ L_v^*+\dfrac{I_{xz}}{I_{xx}}N_v^* & L_p^*+\dfrac{I_{xz}}{I_{xx}}N_p^* & L_r^*+\dfrac{I_{xz}}{I_{xx}}N_r^* & 0 \\ N_v^*+\dfrac{I_{xz}}{I_{zz}}L_v^* & N_p^*+\dfrac{I_{xz}}{I_{zz}}L_p^* & N_r^*+\dfrac{I_{xz}}{I_{zz}}L_r^* & 0 \\ 0 & 1 & 0 & 0 \end{bmatrix} \quad (19)$$

4. Results of Parameter Estimation and Fault Isolation

Tables 3 and 4 show the stability and control derivatives estimated from flight test data for the normal and fault mode by using the Fourier transform regression method. The aerodynamic coefficients computed from the analytical methods of AAA are also included in these tables for the comparison.

Figure 4 shows the comparison of the flight test data and the linear simulation results computed with estimated aerodynamic coefficients.

Table 3 Comparisons of estimated stability & control derivatives

	2-1-1	3-2-1-1	3-2-1-1	3-2-1-1	AAA
	Normal mode		Fault mode		
			0 deg	+5 deg	
TAS	117ft/s	109ft/s	115ft/s	118ft/s	
H	528ft	147ft	352ft	418ft	
C_{D_0}	0.0375	0.1826	0.2087	0.0511	0.0377
C_{D_α}	1.1934	0.7813	1.5649	0.8506	0.1725
C_{L_0}	0.3257	0.3106	0.1576	0.2767	0.6245
C_{L_α}	4.3790	2.8960	1.0823	2.1965	5.5138
$C_{m_{\dot\alpha}}$	−65.8774	−33.8622	−9.4335	−37.9419	−4.0938
C_{m_α}	−1.4103	−1.2037	−1.2517	−1.1563	−1.6219
C_{m_q}	−102.9735	−53.8877	−55.1791	−64.9359	−22.5287
$C_{D_{\delta e}}$	−0.1900	−0.5046	−0.6707	−0.2203	0.0105
$C_{L_{\delta e}}$	−0.4828	−0.4140	−0.9656	−0.5915	0.2649
$C_{m_{\delta e}}$	−1.2644	−0.8794	−0.6275	−0.5334	−1.1879
$C_{l_{\delta e}}$	0.0022	−0.0039	0.0051	0.0011	

Table 4 Comparisons of mean values of estimated stability & control derivatives

	2-1-1	3-2-1-1	3-2-1-1	3-2-1-1	AAA
	Normal mode		Fault mode		
			0 deg	+5 deg	
C_{D_0}	0.1329	0.1107	0.2680	0.0826	0.0377
C_{D_α}	0.3271	0.7265	1.3440	1.6675	0.1725
C_{L_0}	0.2861	0.3666	0.1651	0.2843	0.6245
C_{L_α}	2.8648	3.4217	0.1104	2.0162	5.5138
$C_{m_{\dot\alpha}}$	−37.9412	−48.8353	−38.1488	−31.1830	−4.0938
C_{m_α}	−1.3277	−1.4575	−1.0352	−1.0693	−1.6219
C_{m_q}	−66.0740	−78.0453	−74.6127	−52.5168	−22.5287
$C_{D_{\delta e}}$	−0.0078	−0.1970	−0.5423	−0.3891	0.0105
$C_{L_{\delta e}}$	−1.0448	−0.9802	−1.0897	−0.6162	0.2649
$C_{m_{\delta e}}$	−1.1375	−1.2267	−0.6757	−0.4587	−1.1879
$C_{l_{\delta e}}$	0.0021	0.0006	0.0008	0.0003	

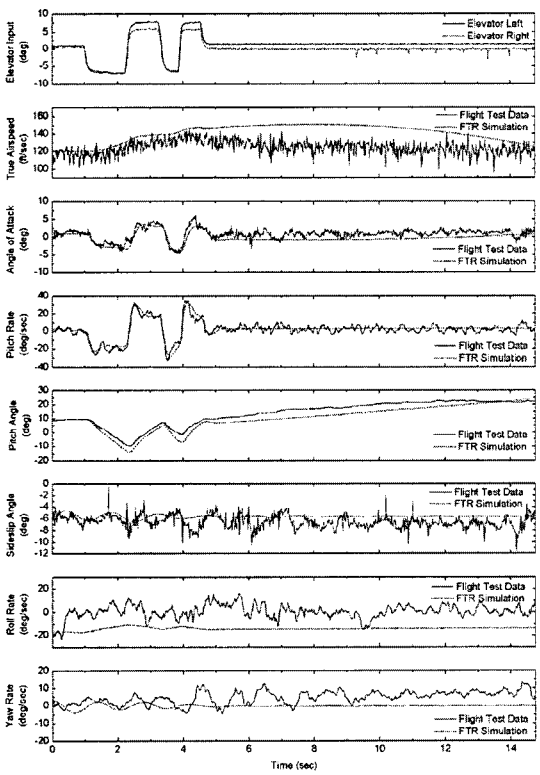

Fig. 4 Results of estimated stability/control derivatives : 3-2-1-1 multi-step input (normal mode)

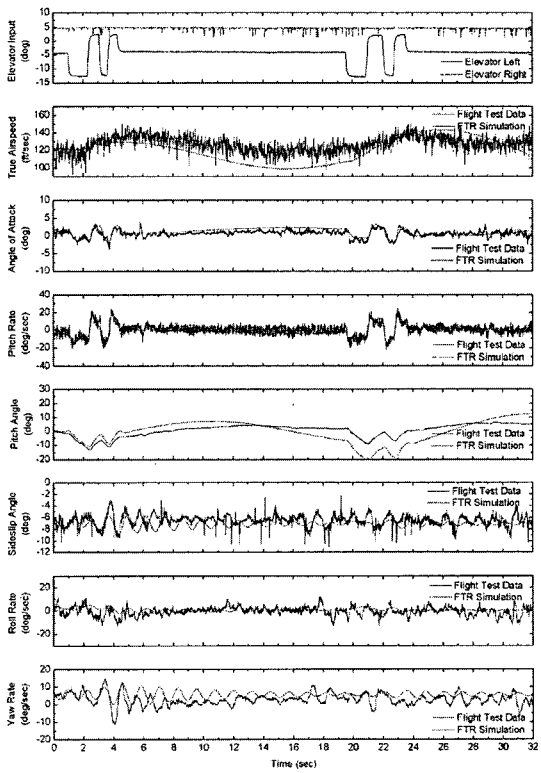

Fig. 5 Results of estimated stability/control derivatives : 3-2-1-1 multi-step input (fault mode)

Fig. 5 shows the flight test data and the linear simulation results for the fault mode. Fig. 6 shows the scatter diagram of the estimated aerodynamic coefficients for several flight cases.

The drag coefficient slop (Smetana, 1983) C_{D_0} computed from the FTR is larger than the result of AAA. The lift coefficient slop C_{L_0} computed from FTR disagrees with AAA. The C_{D_0} and C_{L_0} in Fig. 6 show that the results of normal and fault mode is similar. The C_{m_α} in Fig. 6 shows that the normal and fault state slightly differs from the normal and fault mode. The $C_{m_{\delta e}}$ computed from FTR is similar to AAA in normal mode. The control derivative $C_{m_{\delta e}}$ clearly classifies the difference between the normal and fault mode. Without the relation between the right elevator 0 deg fixed and 5 deg fixed, the malfunction of elevator reduces the elevator effect to a half. The $C_{m_{\delta e}}$ is reduced the malfunction of elevator by half, as shown in Fig. 6.

Fault detection and isolation procedure shows in Fig. 7. Straight level fight trim value of DURUMI-II shows in Table 5. In Mode I case, the system (FCC, Fight Control Computer) recognize as elevator fault that. In Mode II, the system recognize as elevator fault that elevator trim is changed

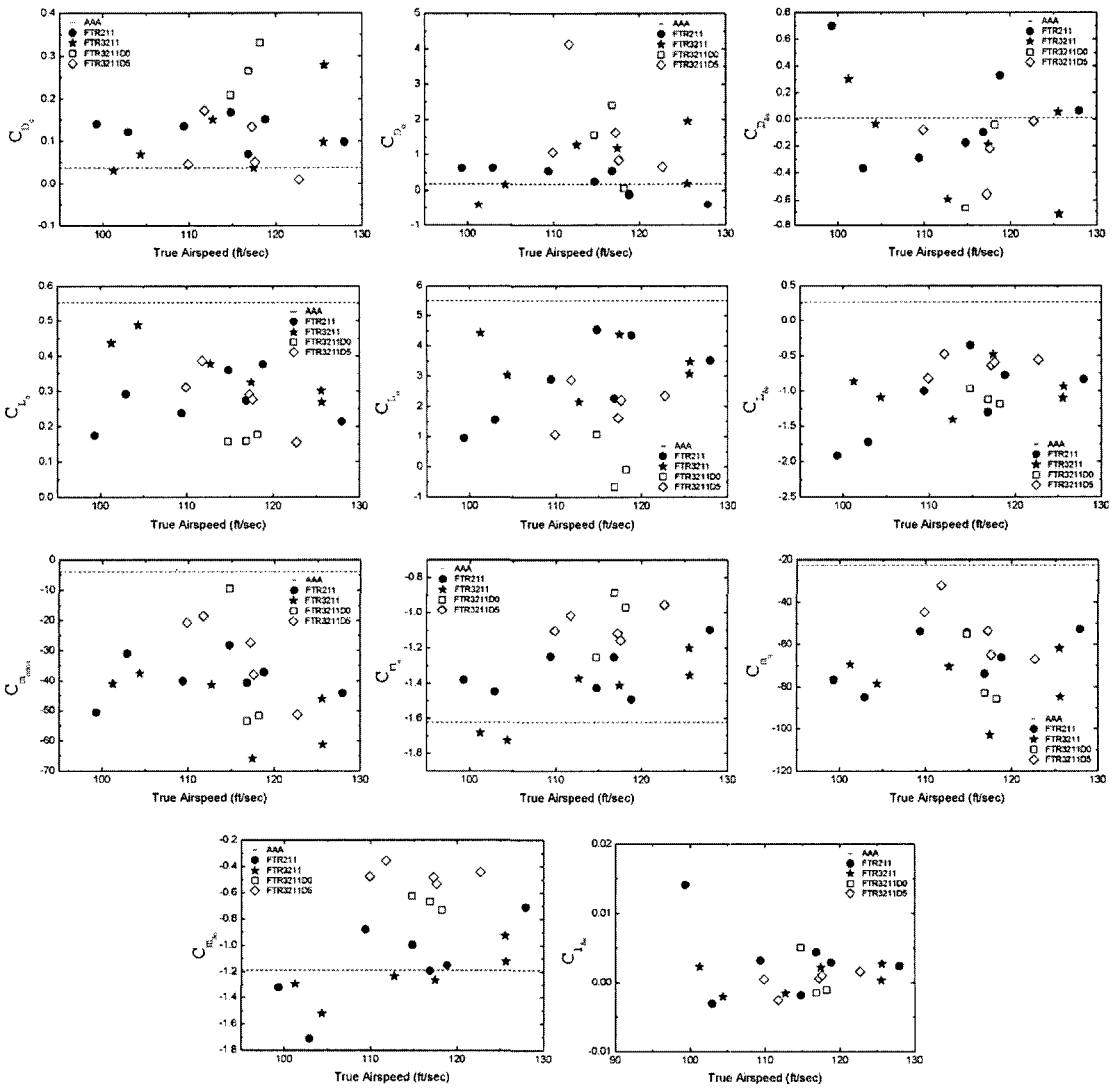

Fig. 6 Scatter diagram of longitudinal coefficients

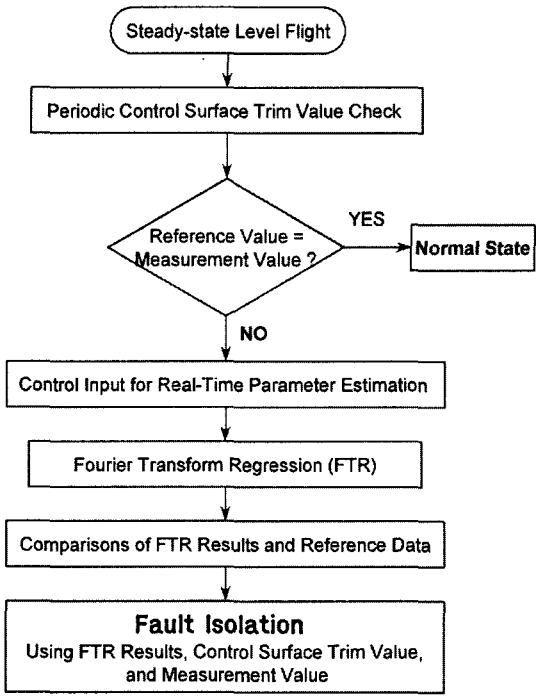

Fig. 7 Fault detection and isolation procedure include autopilot system

Table 5 Straight level flight trim value of normal and fault mode

Trim	Normal Mode	Fault Mode I	Fault Mode II
Elevator (deg)	0.9861	1.4815	4.4312 (up)
Aileron (deg)	−0.3999	−0.4068	−0.3595
Rudder (deg)	0.1736	0.0432	0.2875

and the $C_{m_{\delta e}}$ is only reduced by half. But, the system don't recognize left nor right elevator fault.

5. Conclusions

The fault mode with the fixed right elevator was considered in this paper. The multi-step 3-2-1-1 elevator input for the parameter estimation was implemented successfully in flight by using the programmed switch method. The fault mode was engaged by toggling the 2-pole switch.

The aerodynamic derivatives for DURUMI-II were estimated for the flight test data by using the Fourier transform regression for normal mode and fault mode assumed the right elevator fixed, and were compared with the results from the analytical prediction method. On the whole, The FTR results of the C_{m_α} and $C_{m_{\delta e}}$ from the flight test data in normal mode agree well with the analytical results from AAA. The C_{m_α} in Fig. 6 shows that the normal and fault state slightly differs from the normal and fault mode. The control derivative $C_{m_{\delta e}}$ clearly classifies the difference between the normal mode and the fault mode. The $C_{m_{\delta e}}$ is reduced the malfunction of elevator by half, as shown in Fig. 6. It is not satisfactory to determine the normal and fault state with pattern of C_{m_α}. Therefore, the aerodynamic derivatives of $C_{m_{\delta e}}$ maybe provide the base line of normal/failure for the control surface by using the on-line parameter estimation of Fourier transform regression. In flight, it is capable to detect and isolate the fault of primary control surface. But, the system don't recognize left nor right elevator fault.

For further study, it is desirable to perform more flight test so that the parameter variations could be investigated and analyzed in various failure conditions.

References

FUTABA, 1995, "Futaba Digital Proportional Radio Control Instruction & Operation Manual : PCM1024ZA/PCM1024ZH," FUTABA Corporation.

Garcia-Velo, J. B., 1991, "Parameter Estimation of an Unstable Aircraft Using an Extended Kalman Filter," Master of Science.

Garcia-Velo, J. B. and Walker, B. K., 1997, "Aerodynamic Parameter Estimation for High Performance Aircraft Using Extended Kalman Filter," *J. Guidance, Control and Dynamics*, Vol. 20, No. 6, pp. 1257~1260.

Gelb, A., 1974, "Applied Optimal Estimation," The M.I.T. Press.

Hwang, M. S., Eun, H. B., Park, W. J. et al., 2001, "Lateral Stability/Control Derivatives Estimation of Canard Type Airplane from Flight Test," Proceedings of the ICCAS 2001.

Hwang, M. S., Park, W. J. et al., 2002, "Later-

al Stability Improvement of a Canard Airplane Using a Vertical Panel," AIAA Atmospheric Flight Mechanics Conference and Exhibit, AIAA-2002-4625, Monterey, California.

Ljung, L., 1987, "System Identification : Theory for the User," Prentice Hall, Englewood Cliffs, NJ.

Mendel, J. M., 1987, "Lessons in Digital Estimation Theory," Prentice-Hall.

Morelli, E. A., 1998, "In-flight System identification," Proceedings of the 1998 AIAA Atmospheric Flight Mechanics Conference, AIAA-98-4261, Boston, Ma.

Morelli, E. A., 1999, "Real-Time Parameter Estimation in the Frequency Domain," Proceedings of the 1999 AIAA Atmospheric Flight Mechanics Conference, AIAA-99-4043, Portland, Or.

Morelli, E. A., 2000, "Identification of Low Order Equivalent System Models From Flight Test Data," NASA-TM-210117.

Morelli, E. A., 1997, "High Accuracy Evaluation of the Finite Fourier Transform Using Sampled Data," NASA-TM-110340.

NTPS, 2000, "Introduction to Performance and Flying Qualities Flight Testing," National Test Pilot School.

Napolitano, M. R., Song, Y. K. and Seanor, B., 2001, "On-Line Parameter Estimation for Restructurable Flight Control Systems," Aircraft Design.

Park, W. J., 1997, " Parameter Estimation of Aerodynamic Stability Derivatives Using Extended Kalman Filter (Longitudinal Motion)," Master of Science, Hankuk Aviation University.

Park, W. J., 2004, "A Study on the Design of Real-Time Parameter Estimator for an Aircraft, " PhD Thesis, Hankuk Aviation University.

Smetana, F. O., 1983, "Computer Assisted Analysis of Aircraft-Performance Stability and Control," McGraw-Hill, pp. 37～166.

Song, Y. K., 2001, "A Study on Real-Time Aircraft Parameter Estimation," Proceedings of the KSAS Spring Annual Meeting 2001, pp. 359～362.